TRANSIENT THERMAL STRESSES IN AN INFINITE CLAD SLAB SUBJECTED TO γ-RAY HEATING

Takahito GOSHIMA

Introduction

Clad materials are often used in many pressure vessels of nuclear reactors. Heat is generated in that pressure vessels by absorption of γ-rays which emanate from the core of the reactor. Design of the reactor pressure vessels requires the analysis of the temperature and thermal stresses due to γ-ray radiation. Considerable investigations have been performed on such problems. The thermal stresses in a hollow circular cylinder due to internal heat generation were considered by Kraus et al.[1], Weil[2] and Schmidt et al.[3]. The transient thermal stresses in a slab due to internal heat generation were analyzed by Goshima et al.[4], Singh et al.[5]-[8] and Thomas et al.[9]. However, all these investigations have dealt with the uniform materials. The investigation for a clad material due to γ-ray radiation has been little given in spite of the availability for the nuclear reactor design.

In the present paper, we consider an infinite clad slab subjected to transient internal heat generation decaying exponentially along the slab thickness due to γ-ray radiation on a clad surface, and cooled by convection on both surfaces. The transient temperature and thermal stresses induced in that clad slab are analyzed by making use of Laplace transform and using the Green's function which is the solution for the plane heat source. In the present analysis, it is assumed that the inertia terms in the equilibrium equations are omitted and the properties of the material are independent of temperature. Numerical calculations of the temperature and thermal stress distributions are carried out for the case of the stainless-carbon-steel clad material. The influence of the absorption coefficient, the Biot number and the clad material thickness on the results are considered.

1. Temperature analysis

Consider an infinite clad slad subjected to internal heat generation due to γ-ray radiation and cooled by convection. It is assumed that the strength of γ-ray radiation is constant over the surface of the plate. Therefore, the present analysis is dealt with as two-dimensional problem. Fig. 1 show the geometry and coordinate system for this problem. The base material and the clad material of the clad slab are represented by subscript $j=1$ and 2 respectively. In the present analysis, the following dimensionless parameters and notations are used.

$$\zeta = z/h, \quad \xi = b/h, \quad \eta = a/h, \quad \gamma_j = \mu_j h, \quad \tau = \kappa_1 t/h^2$$

$$B_1 = H_1 h/K_1, \quad B_2 = H_2 h/K_2, \quad \kappa^2 = \kappa_1/\kappa_2, \quad K = K_1/K_2$$

$$T^* = h Q_0/K_1$$

where the definitions of symbols are shown in Nomenclature.

Consider the internal heat generation $Q_j(\zeta, \tau)$ due to γ-ray heating, which is represented by

$$Q_j(\zeta, \tau) = Q_0 f_j(\zeta) H(\tau) \tag{1}$$

where $H(\tau)$ is the Heaviside step function and $f(\zeta)$ is the distribution of internal heat generation.

Supposing that the clad slab is at initial uniform temperature $T_j = O$ and is cooled by convection on it's surface, the initial and the boundary conditions are given as

$$T_j = O \qquad (j = 1, 2) \quad \text{at} \quad \tau = 0 \tag{2}$$

$$\frac{\partial T_1}{\partial \zeta} = -B_1 T_1 \qquad \text{on} \quad \zeta = 1 \tag{3}$$

$$\frac{\partial T_2}{\partial \zeta} = B_2 T_2 \qquad \text{on} \quad \zeta = 0 \tag{4}$$

$$T_1 = T_2 \qquad \text{at} \quad \zeta = \xi \tag{5}$$

$$K \frac{\partial T_1}{\partial \zeta} = \frac{\partial T_2}{\partial \zeta} \qquad \text{at} \quad \zeta = \xi \tag{6}$$

We first consider the temperature field T_j^i due to the plane heat source on $\zeta = \eta$ as shown in fig. 1 with the same initial and boundary conditions as (2)-(6). In this case, $Q(\zeta, \tau)$ represents the heat source per unit time per unit area, and $f_j(\zeta)$ can be expressed as

$$f_j(\zeta) = \delta(\zeta - \eta)/h \tag{7}$$

where $\delta(\zeta - \eta)$ is the Dirac's delta function. Then, the Fourier's heat conduction equation is

$$\frac{\partial^2 T_j^i}{\partial \zeta^2} = \delta \kappa_j \frac{\partial T_j^i}{\partial \tau} - \delta_{kj} \delta_{1j} T^* \delta(\zeta - \eta) \ H(\tau) \tag{8}$$

where

$$\delta \kappa^j = \begin{cases} 1, & j = 1 \\ \kappa^2, & j = 2 \end{cases}$$

$$\delta_{kj} = \begin{cases} 1, & j = 1 \\ K, & j = 2 \end{cases}$$

$$i = \begin{cases} 1, & \xi \leqq \eta \leqq 1 \\ 2, & 0 \leqq \eta \leqq \xi \end{cases}$$

and δ_{ij} is Kronecker delta ($\delta_{ij}=1$ for $i=j$, $\delta_{ij}=0$ for $i \neq j$).　Proceeding in a manner analogous to previous paper[4], the solution of (8) (Green's function), which satisfy the conditions (2)-(6), can be obtained as follows :

$$T^i_j = 2 \sum_{n=1}^{\infty} \frac{(1-e^{-x_n^2 \tau})}{x_n g'(x_n)} G^i_j(\eta) F^i_j(\xi) \tag{9}$$

where

$$G^1_1(\eta) = \begin{cases} KV^c_1(x_n)\cos((\eta-\xi)x_n) + \varkappa V^s_1(x_n)\sin((\eta-\xi)x_n), & \xi > \eta \\ (B_1/x_n)\sin((\eta-1)x_n) - \cos((\eta-1)x_n), & \xi < \eta \end{cases} \tag{10}$$

$$G^1_2(\eta) = K \{(B_1/x_n)\sin((\eta-1)x_n) - \cos((\eta-1)x_n)\} \tag{11}$$

$$G^2_1(\eta) = K \{\cos(\varkappa\eta x_n) + \frac{B_2}{\varkappa x_n}\sin(\varkappa\eta x_n)\} \tag{12}$$

$$G^2_2(\eta) = \begin{cases} (K/\varkappa)V^s_2(x_n)\sin((\eta-\xi)\varkappa x_n) - V^c_2(x_n)\cos((\eta-\xi)\varkappa x_n), & \xi < \eta \\ \cos(\varkappa\eta x_n) + B_2/(\varkappa x_n)\sin(\varkappa\eta x_n), & \xi > \eta \end{cases} \tag{13}$$

$$F^1_1(\xi) = \begin{cases} (B_1/x_n)\sin((\xi-1)x_n) - \cos((\xi-1)x_n), & \xi < \eta \\ KV^c_1(x_n)\cos((\xi-\xi)x_n) + \varkappa V^s_1(x_n)\sin((\xi-\xi)x_n), & \xi > \eta \end{cases} \tag{14}$$

$$F^1_2(\xi) = \cos(\varkappa\xi x_n) + \frac{B_2}{\varkappa x_n}\sin(\varkappa\xi x_n) \tag{15}$$

$$F^2_1(\xi) = \frac{B_1}{x_n}\sin((\xi-1)x_n) - \cos((\xi-1)x_n) \tag{16}$$

$$F^2_2(\xi) = \begin{cases} \cos(\varkappa\xi x_n) + B_2/(\varkappa x_n)\sin(\varkappa\xi x_n), & \xi < \eta \\ (K/\varkappa)V^s_2(x_n)\sin((\xi-\xi)\varkappa x_n) - V^c_2(x_n)\cos((\xi-\xi)\varkappa x_n), & \xi > \eta \end{cases} \tag{17}$$

$$\left. \begin{aligned} V^c_1(x_n) &= \cos(\varkappa\xi x_n) + \frac{B_2}{\varkappa x_n}\sin(\varkappa\xi x_n) \\[6pt] V^s_1(x_n) &= \frac{B_2}{\varkappa x_n}\cos(\varkappa\xi x_n) - \sin(\varkappa\xi x_n) \\[6pt] V^c_2(x_n) &= K\cos((\xi-1)x_n) - \frac{KB_1}{x_n}\sin((\xi-1)x_n) \\[6pt] V^s_2(x_n) &= K\sin((\xi-1)x_n) + \frac{KB_1}{x_n}\cos((\xi-1)x_n) \end{aligned} \right\} \tag{18}$$

and x_n are the positive roots of $g(x_n)=0$

$$g(x) = \{(KB_1 + B_2)\cos(\varkappa\xi x) + (\frac{KB_1B_2}{\varkappa x} - \varkappa x)\sin(\varkappa\xi x)\}$$

$$\times \cos((\xi-1)\mathrm{x})+\ \{(K\mathrm{x}-\frac{B_1 B_2}{\mathrm{x}})\cos(\varkappa\xi\mathrm{x})+(\frac{KB_2}{\varkappa}+B_1\varkappa)$$

$$\times \sin(\varkappa\xi\mathrm{x})\}\ \sin((\xi-1)\mathrm{x}) \tag{19}$$

$$g'(\mathrm{x})=\frac{dg(\mathrm{x})}{d\mathrm{x}}$$

Thus we have gotten the Green's function T^i_j satisfying eq. (8). Therefore, the temperature solution T_j due to the arbitray internal heat generation (1) with the conditions (2)−(6) can be obtained by integrating as

$$\frac{T_j}{T^*}=\int_0^\xi T^2_j f_j(\eta)d\eta+\int_\xi^1 T^1_j f_j(\eta)d\eta \quad (j=1,\ 2) \tag{20}$$

Especially, in case of γ-ray radiation, the heat generation distribution $f_j(\eta)$ is represented as

$$f_j(\xi)=R(\gamma_1,\ \gamma_2)e^{-\gamma_i\xi} \tag{21}$$

Assuming that the whole heat generation per unit time is equal to the plane heat generation per unit time, $R(\gamma_1,\ \gamma_2)$ must be given by,

$$R(\gamma_1,\ \gamma_2)=\gamma_1\gamma_2/\ [\gamma_1(1-e^{-\gamma_2\xi})+\gamma_2(e^{-\gamma_1\xi}-e^{-\gamma_1})] \tag{22}$$

Substituting eqs. (21) and (9) into eq. (20), we can get the solution of the temperature T_j due to γ-ray heating as

$$\frac{T_j}{T^*}=2R(\gamma^1,\ \gamma^2)\sum_{n=1}^\infty \frac{(1-e^{-x_n^2\tau})}{x_n g'(x_n)}\sum_{i=1}^2\ \{F^i_j(\xi)W^i_j(\xi)\} \quad (j=1,\ 2) \tag{23}$$

$$W^1_j(\xi)=\int_\xi^1 G^1_j(\eta)e^{-\gamma_i\eta}d\eta$$

$$\qquad\qquad (j=1,\ 2) \tag{24}$$

$$W^2_j(\xi)=\int_0^\xi G^2_j(\eta)e^{-\gamma_i\eta}d\eta$$

2. Stress analysis

In the clad slab, the thermal stresses are caused not only by the temperature distribution but also by interactive restraining in construction between clad and base materials. Denoting the interacting force and bending moment per unit length N_x and M_j respectively as fig. 2, the thermal stressen caused in the clad slab are given as[10]

$$\frac{1-v_1}{E_1\alpha_1 T^*}\sigma_x=-\frac{N_x}{1-\xi}+\frac{12M_1}{(1-\xi)^3}(\zeta-\frac{1+\xi}{2})+I^n_1$$

$$+\frac{2}{1-\xi}(\zeta-\frac{1+\xi}{2})I^m_1-\frac{T_1}{T^*},\ (\xi\leqq\zeta\leqq1) \tag{25}$$

$$\frac{1-v_2}{E_2\alpha_2 T^*}\sigma_x = \frac{N_x}{\xi} + \frac{12M_2}{\xi^3}(\zeta - \frac{\xi}{2}) + I^n_2$$

$$+ \frac{2}{\xi}(\zeta - \frac{\xi}{2})I^m_2 - \frac{T_2}{T^*},$$

$$(0 \leq \zeta \leq \xi) \qquad (26)$$

where

$$I^n_1 = \frac{1}{1-\xi}\int_\xi^1 \frac{T_1}{T^*}d\zeta$$

$$I^n_2 = \frac{1}{\xi}\int_0^\xi \frac{T_2}{T^*}d\zeta \qquad (27)$$

$$I^m_1 = \frac{6}{(1-\xi)^2}\int_\xi^1 \frac{T_1}{T^*}$$

$$(\zeta - \frac{1+\xi}{2})d\zeta$$

$$I^m_2 = \frac{6}{\xi^2}\int_0^\xi \frac{T_2}{T^*}(\zeta - \frac{\xi}{2})d\zeta$$

Fig. 1. Geometry and coordinate system

Considering the clad slab free from external force, the equation of equilibrium is

$$M_1 + M_2 - \frac{h}{2}N_x = 0 \qquad (28)$$

The continuous conditions on the splicing surface, in the x-direction strain and in the z-direction displacement, are shown as

$$-\frac{(1-v_1)}{E_1}\{\frac{N_x}{1-\xi} + \frac{6M_1}{(1-\xi)^2}\} + \alpha_1(I^n_1 - I^m_1)$$

$$= \frac{(1-v_2)}{E_2}(\frac{N_x}{\xi} + \frac{6M_2}{\xi^2}) + \alpha_2(I^n_2 + I^m_2) \qquad (29)$$

$$\frac{2\alpha_1}{1-\xi}I^m_1 + \frac{12(1-v_1)}{(1-\xi)^3 E_1}M_1 = \frac{2\alpha_2}{\xi}I^m_2 + \frac{12(1-v_2)}{\xi^3 E_2}M_2 \qquad (30)$$

N_x, M_1, M_2 in eqs. (25) and (26) are easily determined by eqs. (28)−(30).
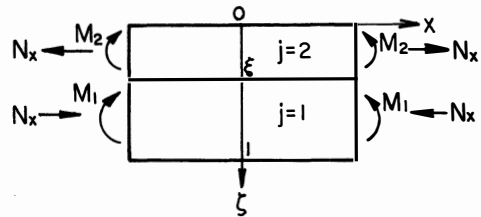
Fig. 2. Interacting force and bending moment

3. Numerical calculations

Numerical calculations are carried out for the case of the stainless-carbon-steel clad material. The material constants are shown in table 1. We assumed that the absorption coefficients of γ -ray energy are in the relation of $\mu_1 = \mu_2 = \mu$ or $\gamma_1 = \gamma_2 = \gamma$.

Figs. 3 and 4 show the temperature and stress distributions through slab thickness for various values of dimensionless time τ, with $\gamma = 10$, $B_1 = 0$, $B_2 = 10$ and $\xi = 0.2$. When $\tau \leq 0.5$ the maximum tensile stress occurs on the splicing surface in the base material ($\zeta = \xi^{+0}$). However, when $\tau > 0.5$ the tensile stress show the maximum value at the surface of the clad material ($\zeta = 0$) and the maximum compressive stress occurs on the splicing surface in the clad material ($\zeta = \xi^{-0}$).

Figs. 5 and 6 show the effects of the clad surface convective cooling on the temperature and stress distributions in the case of $B_1 = 0$, $\gamma = 10$, $\tau = 0.1$ and $\xi = 0.2$. When at least $B_2 \leq 10$ the maximum tensile stress occurs on the splicing surface in the base material ($\zeta = \xi^{+0}$), but when $B_2 = \infty$ the tensile stress show the maximum value at the surface of the clad material ($\zeta = 0$). While, the maximum compressive stress always occurs in the clad material ($0 \leq \zeta \leq \xi$). Fig. 7 shows the stress variations at the clad surface ($\zeta = 0$) for various values of B_2 with $B_1 = 0$, $\gamma = 10$, $\xi = 0.2$. It can be seen that the steady states are reached rapidly with the increase of B_2. For example, when $B_2 = \infty$ the steady state is reached at $\tau > 3$.

Figs. 8 and 9 show the temperature and stress distributions for various values of dimensionless γ-ray absorption coefficient γ, with $B_1 = 0$, $B_2 = 10$, $\tau = 0.1$ and $\xi = 0.2$. When $\gamma \geq 5$ the maximum tensile stress occurs on the splicing surface in the base material ($\zeta = \xi^{+0}$). However, when $\gamma \leq 1$ the maximum tensile stress occurs at the clad surface ($\zeta = 0$) and the maximum compressive stress occurs on the splicing surface in the clad material ($\zeta = \xi^{-0}$). Fig.10 shows the stress variations at the clad surface ($\zeta = 0$) for various values of γ with $B_1 = 0$, $B_2 = 10$ and $\xi = 0.2$. It can be seen that when $\tau < 10$ the steady states are reached approximately independently of the value of γ.

Finally, figs. 11-14 show the effects of the clad thickness on the temperature and stress distributions for two cases of $\tau = 0.1$ and ∞, with $B_1 = 0$, $B_2 = 10$, $\gamma = 10$. For $\tau = 0.1$ (fig. 12), when $\xi \leq 0.1$ the maximum tensile stress occurs inside of the base material ($\zeta \fallingdotseq 0.5$), but when $\xi \geq 0.2$ the maximum tensile stress occurs on the splicing surface in the base material ($\zeta = \xi^{+0}$). While, for $\tau = \infty$ (fig. 14), when $\xi \leq 0.05$ the maximum tensile stress occurs on the splicing surface in the base material ($\zeta = \xi^{+0}$), but when $\xi \geq 0.1$ the maximum tensile stress occurs at the clad surface ($\zeta = 0$).

Table 1. Material constants of clad slab

	clad material (j = 2) stainless-steel	base material (j = 1) carbon-steel
α_j	17.9×10^{-6} /°C	12.2×10^{-6} /°C
E_j	193 GPa	207 GPa
K_j	16.3 W/(mK)	53.4 W/(mK)
κ_j	4.4×10^{-6} m²/s	14.7×10^{-6} m²/s
ν_j	0.3	0.3
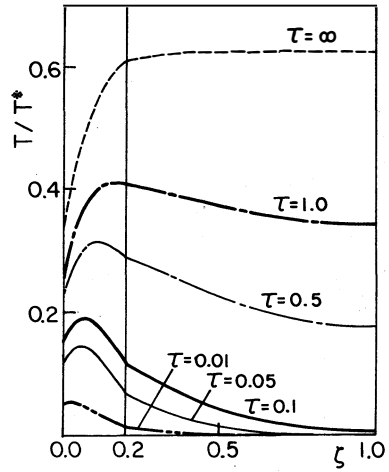
Fig. 3. Temperature distributions for various values of dimensionless time τ for the case $\gamma = 10$, $B_1 = 0$, $B_2 = 10$ and $\xi = 0.2$.
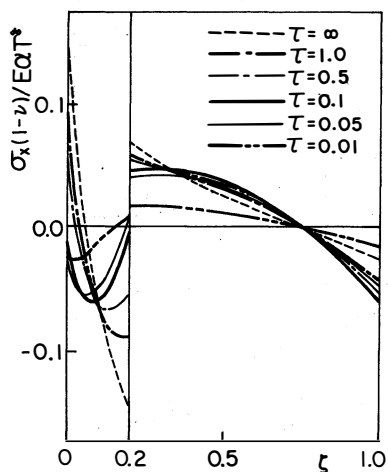
Fig. 4. Thermal stress distributions for various values of dimensionless time τ for the case of $\gamma = 10$, $B_1 = 0$, $B_2 = 10$ and $\xi = 0.2$.
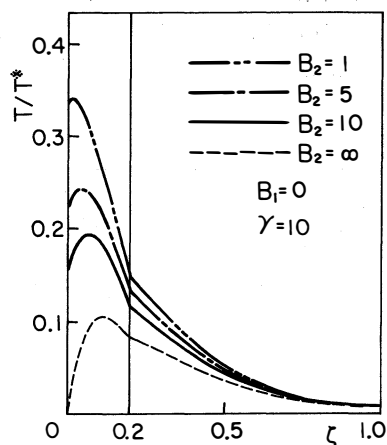
Fig. 5. Temperature distributions showing effect of the Biot number B_2 for the case of $\gamma = 10$, $B_1 = 0$, $\tau = 0.1$ and $\xi = 0.2$.
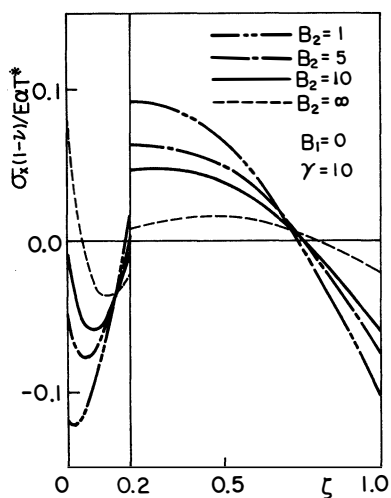
Fig. 6. Thermal stress distributions showing effect of the Biot number B_2 for the case of $\gamma = 10$, $B_1 = 0$, $\tau = 0.1$ and $\xi = 0.2$.
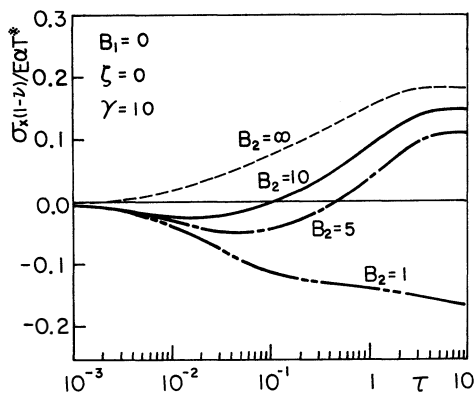
Fig. 7. Thermal stress variations at the clad surface for various values of the Biot number B_2 with $\gamma = 10$, $B_2 = 0$ and $\xi = 0.2$.
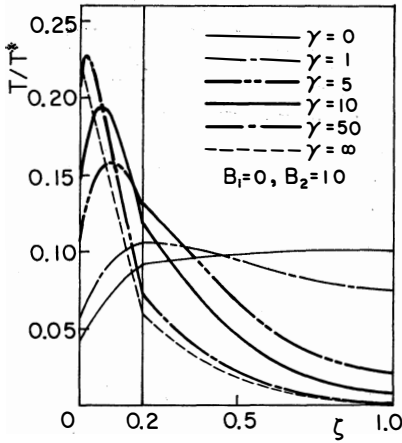
Fig. 8. Temperature distributions showing effect of the dimensionless absorption coefficient γ for the case of $B_1=0$, $B_2=10$, $\tau=0.1$ and $\xi=0.2$.
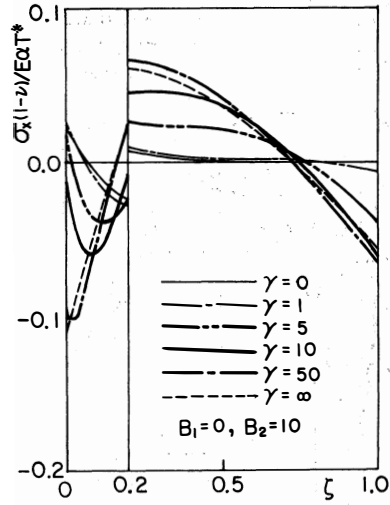
Fig. 9. Thermal stress distributions showing effect of the dimensionless absorption coefficient γ for the case of $B_1=0$, $B_2=10$, $\tau=0.1$ and $\xi=0.2$.
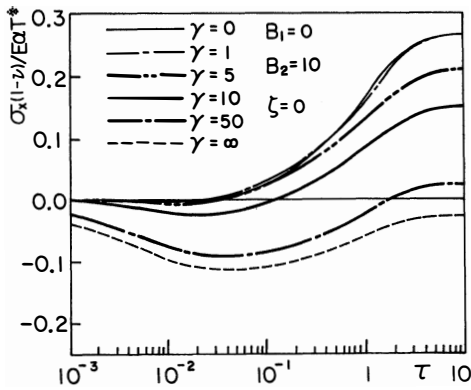
Fig. 10. Thermal stress variations at the clad surface for various values of the dimensionless absorption coefficient γ with $B_1=0$, $B_2=10$ and $\xi=0.2$.
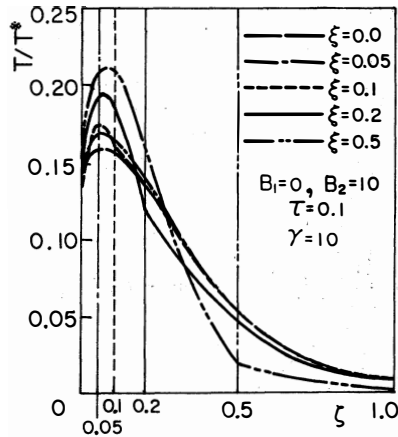
Fig. 11. Temperature distributions showing effect of the clad thickness ξ for the case of $\tau=0.1$ with $B_1=0$, $B_2=10$ and $\gamma=10$.
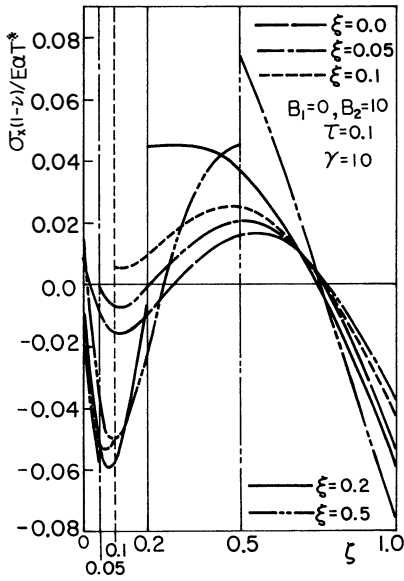
Fig. 12. Thermal stress distributions showing effect of the clad thickness ξ for the case of $\tau = 0.1$ with $B_1 = 0$, $B_2 = 10$ and $\gamma = 10$.
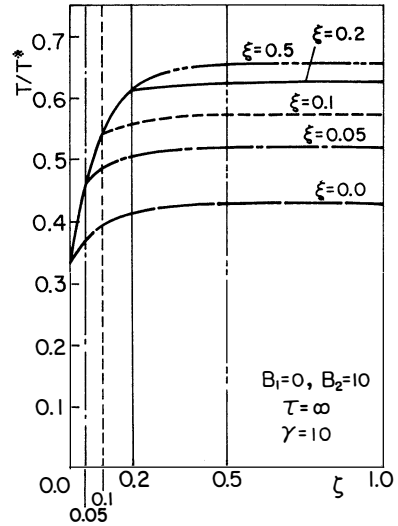
Fig. 13. Temperature distributions showing effect of the clad thickness ξ for the case of $\tau = \infty$ with $B_1 = 0$, $B_2 = 10$ and $\gamma = 10$.
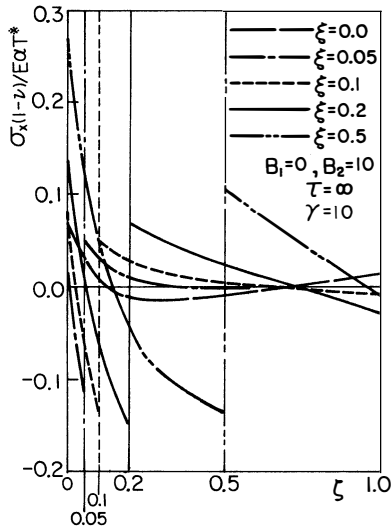
Fig. 14. Thermal stress distributions showing effect of the clad thickness ξ for the case of $\tau = \infty$ with $B_1 = 0$, $B_2 = 10$ and $\gamma = 10$.

Nomenclature

T_j	=	temperature
σ_x	=	thermal stress
h	=	slab thickness
b	=	clad thickness
(x, z)	=	cartesian coordinates (fig. 1)
a	=	location of plane heat source (fig. 1)
t	=	time
μ_j	=	absorption coefficient for γ-ray energy
α_j	=	coefficient of thermal expansion
E_j	=	Young's modulus
K_j	=	thermal conductivity
$\varkappa_j$	=	thermal diffusivity
ν_j	=	Poisson's ratio
H_j	=	coefficient of heat transfer at both surfaces
Q_0	=	heat source density per unit time per unit volume
ζ	=	dimensionless depth (z/h)
ξ	=	dimensionless clad thickness (b/h)
η	=	dimensionless location of plane heat source (a/h)
τ	=	dimensionless time (Fourier number)
B_j	=	Biot number at both surfaces
γ_j	=	dimensionless absorption coefficient of γ-ray ($\mu_j h$)
$\varkappa^2$	=	ratio of thermal diffusivity ($\varkappa^2 = \varkappa_1/\varkappa_2$)
K	=	ratio of thermal conductivity ($K = K_1/K_2$)
j	=	1(base material), 2(clad material)

Reference

(1) H. Kraus and G. Sonnemann : *Trans. ASME J. Eng. for Power*, **81**, 449(1959)

(2) N.A. Weil : *Trans. ASME J. Eng. for industry*, **84**, 35(1962)

(3) J.E. Schmidt and G. Sonnemann : *Trans. ASME J. Heat Transfer*, **82**, 273(1960)

(4) T. Goshima, T. Koizumi and I. Nakahara : *Nuclear Eng. Design*, **31**, 77(1974)

(5) J.P. Singh, J. R. Thomas Jr. and D. P. H. Hasselman : *J. Thermal Stresses*, **3**, 341(1980)

(6) J.P. Singh, J.R. Thomas Jr. and D.P.H. Hasselman : *J. Thermal Stresses*, **6**, 93(1983)

(7) J.P. Singh, J.R. Thomas Jr. and D.P.H. Hasselman : *J. Thermal Stresses*, **6**, 355(1983)

(8) J.P. Singh, J.I. Frankel, J.R. Thomas Jr. and D.P.H. Hasselman : *J. Thermal Stresses*, **6**, 25(1983)

(9) J.R. Thomas Jr., J.P. Singh and D. P.H. Hasselman : *J. Thermal Stresses*, **5**, 247(1982)

(10) R.B. Hetnarski, *Thermal Stresses I*, P. 23, North-Holland, amsterdam, (1977)

TRANSIENT THERMAL STRESSES IN AN INFINITE CLAD SLAB SUBJECTED TO $\gamma-$RAY HEATING

Takahito GOSHIMA

Transient temperature and thermal stresses distributions arising in an infinite clad slab subjected to internal heat generation decaying exponentially along the thickness due to γ-ray radiation are analyzed with the thermal condition of cooling by convention on both surfaces. Numerical calculations of the transient temperature and thermal stress distributions are carried out for the case of the stainless-carbon-steel clad material. The influence of the absorption coefficient, the Biot number and the clad thickness on the results are cosideredz

〔英文和訳〕

ガンマ線加熱を受けるクラッド 無限板に生ずる非定常熱応力

五　嶋　孝　仁

　無限に広いクラッド厚板が，γ線放射により板厚方向に指数関数状に減衰する内部熱発生によって加熱されるとき，生ずる非定常温度場と非定常熱応力分布を，両表面が熱伝達によって冷却されているという熱的条件のもとに解析した。とくにステンレス―炭素鋼のクラッド材について，非定常温度と非定常熱応力分布の数値計算を行ない，吸収係数やビオ数及びクラッド厚さが結果に及ぼす影響を検討した。